Multifunctional Nanoparticles for Combined Doxorubicin and Photothermal Treatments

Huiyul Park,[†,‡] Jaemoon Yang,[§,⊥] Jaemin Lee,[⊥] Seungjoo Haam,[†,⊥] In-Hong Choi,[†,¶] and Kyung-Hwa Yoo[†,‡,*]

[†]National Core Research Center for Nanomedical Technology, Yonsei University, Seoul 120-749, Korea, [‡]Department of Physics, Yonsei University, Seoul 120-749, Korea, [§]Department of Radiology, College of Medicine, Yonsei University, Seoul 120-752, Korea, [⊥]Department of Chemical and Biomolecular Engineering, Yonsei University, Seoul 120-749, Korea, and [¶]Department of Microbiology, Yonsei University, Seoul 120-749, Korea

ABSTRACT To facilitate combined doxorubicin and photothermal treatments, we developed doxorubicin-loaded poly(lactic-*co*-glycolic acid)-gold half-shell nanoparticles (DOX-loaded PLGA—Au H-S NPs) by depositing Au films on DOX-loaded PLGA NPs. As the PLGA NPs biodegraded, DOX was released, and heat was locally generated upon near-infrared (NIR) irradiation due to NIR resonance of DOX-loaded PLGA H-S NPs. Compared with chemotherapy or photothermal treatment alone, the combined treatment demonstrated a synergistic effect, resulting in higher therapeutic efficacy and shorter treatment times. Since our NPs selectively deliver both heat and drug to tumorigenic regions, they may improve the therapeutic effectiveness with minimal side effects.

KEYWORDS: chemo-photothermal treatment · NIR resonance · doxorubicin · synergistic effect

The therapeutic efficacy of chemotherapeutic agents largely depends on adequate local delivery to the tumor site. Most chemotherapeutic agents show a high efficacy with a variety of solid tumors.[1−3] However, nonspecific delivery leads to significant normal tissue toxicities and limits dosages of anticancer drugs to levels far below those required to destroy most malignant lesions. To overcome these problems, various targeted drug deliveries[4] and combined treatments[5−7] to enhance the cytotoxic effect of chemotherapeutic agents have been studied. One combined treatment with chemotherapy is thermochemotherapy. Heat treatment, called hyperthermia, has been demonstrated to augment the cytotoxicity of some chemotherapeutic agents, resulting in the same results with lower doses of the drug.[8−10] In traditional thermochemotherapy, however, the heat is usually provided by hot water baths,[11] microwave,[12] and ultrasound,[13] so that undesirable side effects are often caused due to nontargeted heating.

Recently, near-infrared (NIR) resonant nanomaterials such as gold (Au) nanoshell particles,[14−16] Au nanocages,[17,18] Au nanorods,[19,20] and single-walled carbon nanotubes,[21,22] have been widely studied as heat carriers for local heating. These materials strongly absorb NIR light and convert it into cytotoxic heat; thus, they can be utilized for tumor-selective treatments.[17−21] In addition, nanomaterial-based hyperthermia can be combined with chemotherapy, as in traditional thermochemotherapy. T. S. Hauck

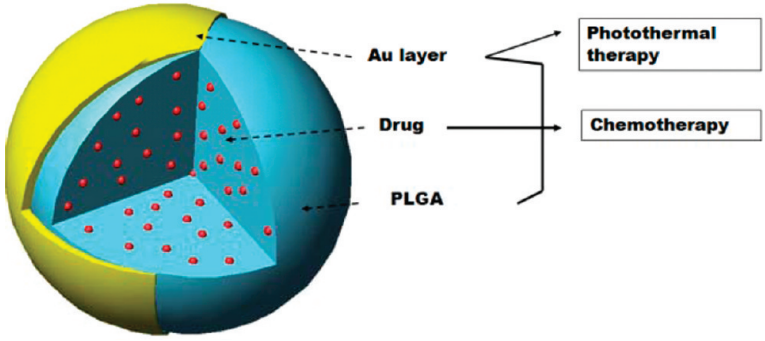

Figure 1. Schematic diagram of DOX-loaded PLGA—Au H-S NPs. The drug is encapsulated within biocompatible and biodegradable PLGA NPs, and a Au layer is deposited on these NPs. Since these NPs are NIR resonant and PLGA is biodegradable, heat is generated upon NIR irradiation and the drug loaded in the PLGA NPs is released through the open half of the shell when the interior is exposed.

*Address correspondence to khyoo@yonsei.ac.kr.

Received for review March 4, 2009 and accepted September 13, 2009.

Published online September 22, 2009.
10.1021/nn900215k CCC: $40.75

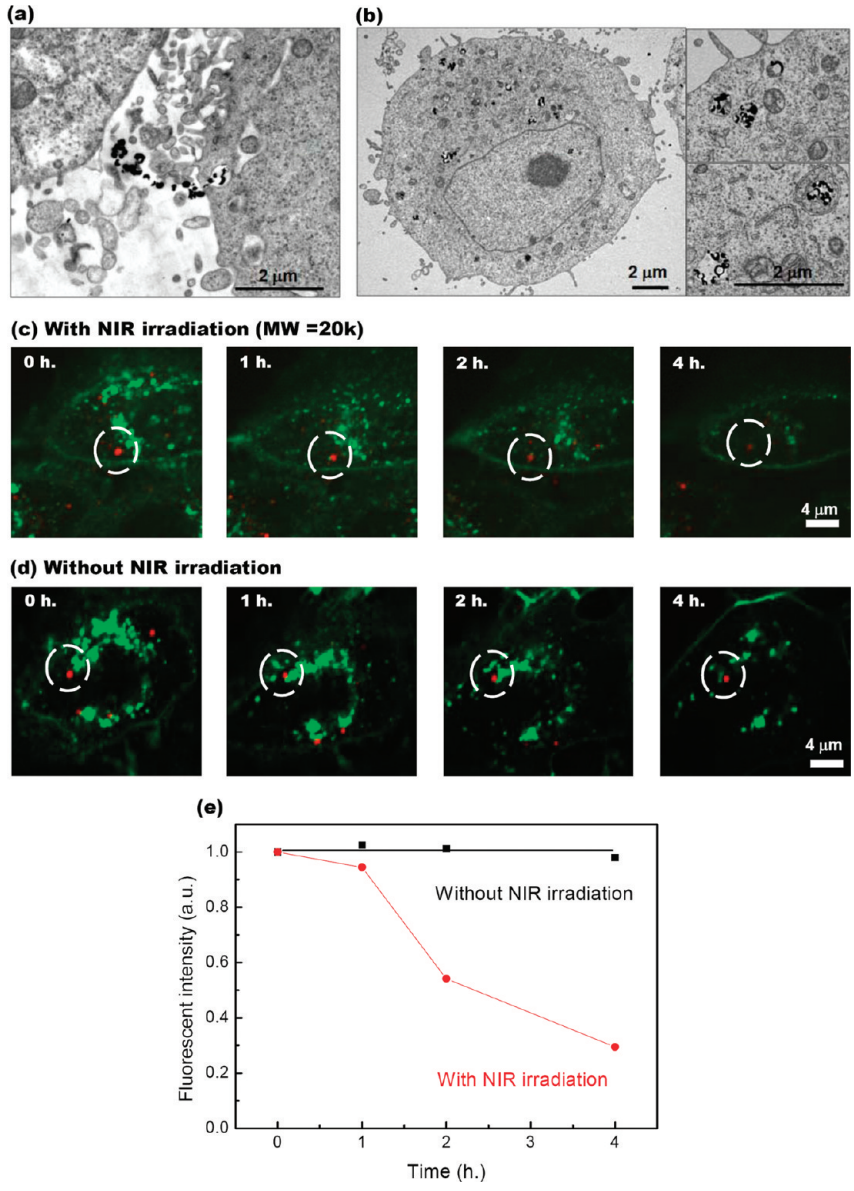

Figure 2. (a) TEM image of HeLa cells incubated with PLGA−Au H-S NPs taken at the moment of endocytosis. (b) TEM image of HeLa cell with PLGA−Au H-S NPs accumulated in vesicles and organelles. Time lapse confocal images of rhodamine-loaded PLGA (M_w = 20000)−Au H-S NPs taken up into a HeLa cell with 0.7 W/cm^2 NIR irradiation (c) and without NIR irradiation (d). The red spot marked by a white circle corresponds to rhodamine-loaded PLGA−Au H-S NPs. (e) Fluorescent intensity of rhodamine time estimated from the data in Figure 2c,d.

et al. combined Au nanorod hyperthermia with chemotherapeutic drugs and demonstrated a superadditive or synergistic effect.[23] However, nanomaterial-based hyperthermia delivers only the heat to the tumorigenic region and not the drugs. If both heat and drugs can be delivered simultaneously to the tumorigenic region, the therapeutic efficacy is expected to be significantly improved with minimal side effects. Therefore, treatments that deliver both heat and drugs simultaneously to the tumorigenic region are highly desirable.

Here, we report the use of drug-loaded poly(lactic-*co*-glycolic acid)−Au half-shell nanoparticles (PLGA−Au H-S NPs) (Figure 1) for tumor-specific delivery of heat and drugs in human cervical cancer (HeLa) cell line. The drug is encapsulated within biocompatible and biodegradable PLGA NPs, and a Au layer is deposited on these NPs. Since these NPs are NIR resonant and PLGA is biodegradable,[24] heat is generated upon NIR irradiation and the drug loaded in the PLGA NPs is released through the open half of the shell when the interior is exposed. Furthermore, it is possible to increase the rate of drug release by NIR irradiation, because PLGA is degraded more rapidly at elevated temperatures. In this study, we used doxorubicin as a chemotherapeutic agent and compared the combined treatment of doxorubicin and NIR irradiation with chemo- or photothermal treatment alone. The chemo-photothermal treatments exhibited a clear synergistic effect.

RESULTS AND DISCUSSION

Prior to the experiments with doxorubicin (DOX)-loaded PLGA−Au H-S NPs, we prepared PLGA−Au H-S NPs with no drug and PLGA (M_w = 20000)−Au H-S NPs containing rhodamine as a model drug and investigated their behavior in HeLa cells. Figure 2 panels a and b show transmission electron microscope (TEM) images of HeLa cells incubated in medium containing PLGA−Au H-S NPs (30 μg/cm^2) for ~4 to 12 h, in which 30 μg/cm^2 was calculated using the relation of NPs concentration (100 μg/mL) × added volume (3 mL)/bottom area of culture well (9.6 cm^2). NPs were taken up by the cell *via* endocytosis and accumulated within vesicles, although some NPs were found inside an organelle enclosed by a bilayer. Figure 2 panels c and d present the time-lapse images, captured using a confocal microscope of HeLa cells treated with rhodamine-loaded PLGA−Au H-S NPs (17.7 μg/cm^2 ≈ 100 μg/mL × 200 μL/1.13 cm^2) with and without NIR irradiation of 0.7 W/cm^2. The intensity of the red spot (marked by a white circle) decreased during NIR irradiation, while it remained nearly unchanged in the absence of NIR irradiation, indicating that the drug was released more rapidly with NIR irradiation (Figure 2e).

Next, we fabricated DOX-loaded PLGA−Au H-S NPs using PLGA with the molecular weight of 5000. According to the results shown in Figure 2 panels d and e, rhodamine was not nearly released within 4 h without NIR irradiation, so that we lowered the molecular

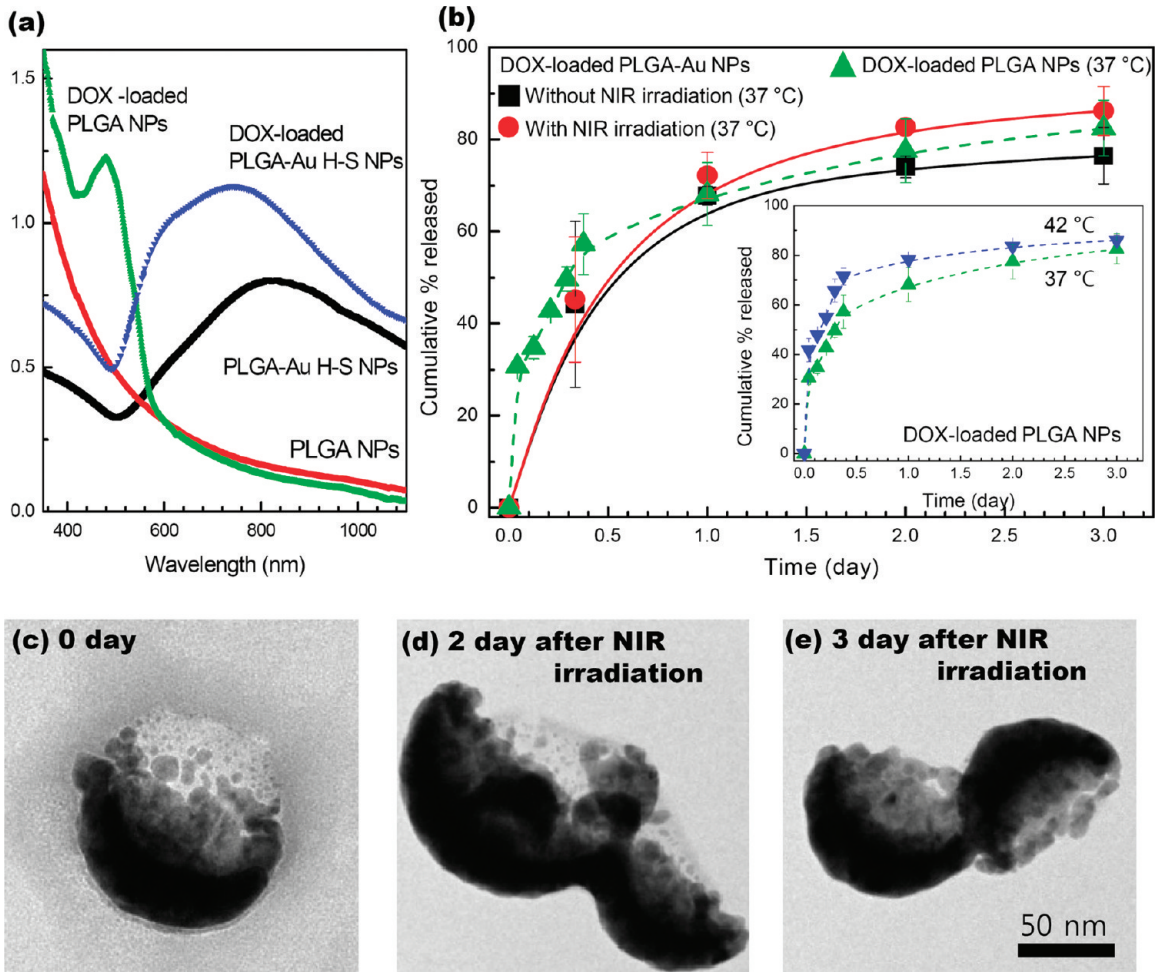

Figure 3. (a) Visible/NIR absorption spectra of PLGA NPs, DOX-loaded PLGA NPs, PLGA−Au H-S NPs, and DOX-loaded PLGA−Au H-S NPs. (b) DOX release profiles from DOX-loaded PLGA (M_W = 5000)−Au H-S NPs without and with NIR irradiation. The inset shows the release profiles from DOX-loaded PLGA NPs at 37 and 42 °C. TEM images of a DOX-loaded PLGA−Au H-S NP as prepared (c), and irradiated by 1.5 W/cm^2 NIR for 4 min and then left in water for 2 days (d) and 3 days (e).

weight of PLGA to enhance the rate of drug release.[26] Figure 3a depicts the absorption spectra measured using a ultraviolet−visible/NIR spectrometer for PLGA−Au H-S NPs and DOX-loaded PLGA−Au H-S NPs. DOX-loaded PLGA−Au H-S NPs revealed a pronounced surface plasmon resonance absorption in the NIR region, although compared with PLGA−Au NPs without DOX ($\lambda \approx 800$ nm), the absorption peak of DOX-loaded PLGA−Au NPs was slightly shifted to the shorter wavelength ($\lambda \approx 790$ nm) presumably owing to loaded DOX, whose absorption peak was located at $\lambda \approx 490$ nm.

To estimate how fast DOX is released from DOX-loaded PLGA−Au H-S NPs, we measured the release profile at 37 °C, as shown in Figure 3b. Since the molecular weight of PLGA was low, DOX was released rapidly and about 68% of DOX loaded in PLGA NPs came out in 1 day without showing lag phase and zero order release that belong to the typical triphasic profile of PLGA particles. For comparison, we also measured the release profile of DOX-loaded PLGA NPs without Au half-shells at 37 and 42 °C (inset of Figure 3b). As expected, DOX came out more rapidly from DOX-loaded PLGA NPs than from DOX-loaded PLGA−Au H-S NPs, and its rate was further enhanced at 42 °C. Moreover, the release profiles of DOX-loaded PLGA−Au H-S NPs obtained without and with NIR irradiation are compared in Figure 3b, where DOX loaded PLGA−Au H-S NPs was initially irradiated by 1.5 W/cm^2 NIR during 4 min and thereafter maintained at 37 °C. Despite the short irradiation time, more DOX was released upon NIR irradiation.

In addition to *in vitro* release experiments, we further studied the morphology of DOX loaded PLGA−Au H-S NP using TEM. A TEM image of DOX loaded PLGA−Au H-S NP as prepared is presented in Figure 3c. A half-shell structure was clearly seen. Figure 3 panels d and e show TEM images of DOX loaded PLGA−Au H-S NP irradiated by 1.5 W/cm^2 NIR during 4 min and then left in water at 37 °C for 2 and 3 days, respectively. After 3 days, the PLGA uncovered with Au was completely degraded, and only Au H-S NPs are left. This finding is consistent with the *in vitro* release experiments in Figure 3b.

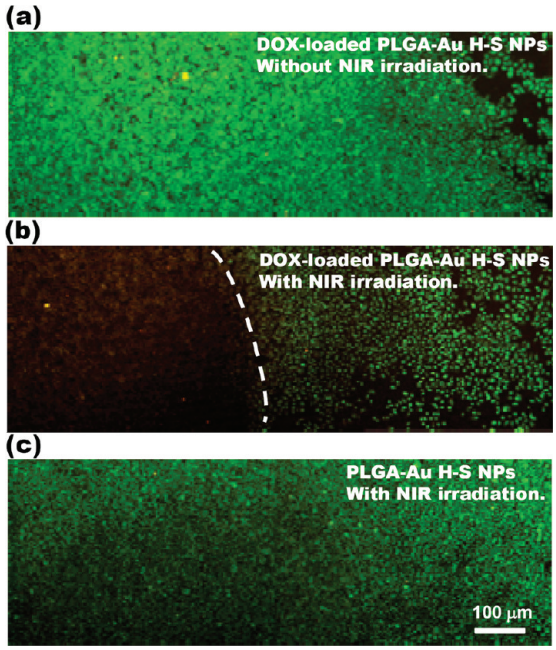

Figure 4. Fluorescence microscope images of HeLa cells treated with DOX-loaded PLGA−Au H-S NPs for 1 d without NIR irradiation (a) and with 0.7 W/cm^2 NIR irradiation for 10 min (b). The dashed curve indicates the region exposed by NIR light. (c) Fluorescence microscope image of HeLa cells incubated with PLGA−Au H-S NPs containing no doxorubicin and then irradiated with 0.7 W/cm^2 NIR light for 10 min.

To investigate the chemo-photothermal treatment, we treated HeLa cells with DOX-loaded PLGA−Au H-S NPs. Then, the cell viability was measured with and without NIR irradiation by staining cells with calcein-AM green fluorescent dye. Figure 4a shows a fluorescence microscope image of HeLa cells incubated with DOX-loaded PLGA−Au H-S NPs (70.8 μg/cm^2 ≈ 400 μg/mL × 200 μL/1.13 cm^2) for 1 d; we estimated that approximately 575 nM doxorubicin was contained within 70.8 μg/cm^2 DOX-loaded PLGA−Au H-S NPs. Although HeLa cells were exposed to doxorubicin, we found that most of the cells were alive because of the low doxorubicin dose. Figure 4b shows a fluorescence microscope image of HeLa cells incubated with DOX-loaded PLGA H-S NPs (70.8 μg/cm^2) for 1 d and then irradiated with 0.7 W/cm^2 NIR for 10 min. In contrast with the result obtained without NIR irradiation (Figure 4a), a dark region is clearly present, indicating that the cells exposed to NIR were dead, whereas the cells not exposed to NIR were alive. To determine whether the cell death observed in Figure 4b was induced by NIR irradiation alone or the combined effects of doxorubicin and NIR irradiation, HeLa cells were also incubated with PLGA H-S NPs (70.8 μg/cm^2) without doxorubicin for 1 d and then irradiated by 0.7 W/cm^2 NIR for 10 min, as in Figure 4b. As shown in Figure 4c, most of the cells appeared to be alive, although the green fluorescence emission was slightly lower. From these results, we conclude that combined doxorubicin and photothermal treatment is more cytotoxic than chemotherapy or photothermal treatment alone. We propose two possible origins for this synergistic effect. First, the cytotoxicity of doxorubicin is enhanced by increasing the temperature, as reported by others.[8−10,27] Second, cells exposed to doxorubicin are more sensitive to heat than are cells not exposed to doxorubicin, so that the cells exposed to doxorubicin are killed by the lower heat.

For more quantitative evaluation of therapeutic efficacy, we measured the viability of treated HeLa cells using cell-counting kit-8 (CCK-8). In Figure 5a, the measured viability is plotted as a function of incubation time for HeLa cells treated with different concentrations of DOX-loaded PLGA H-S NPs (60, 120, and 180 μg/cm^2),[25] where 0.65, 1.3, and 1.95 μM doxorubicin were estimated to be contained in 60, 120, and 180 μg/cm^2 DOX-loaded PLGA−Au H-S NPs, respectively. For the control experiment, the cells were incubated with PLGA−Au H-S NPs (180 μg/cm^2) containing no doxorubicin. No cytotoxicity was observed in the cells treated with PLGA−Au H-S NPs, indicating that PLGA H-S NPs were biocompatible. However, when cells were incubated with DOX-PLGA H-S NPs, the viability decreased to ~60 to 80% after 1 d, depending on the particle concentration, and decreased further with increasing the incubation time. In addition, we also treated HeLa cells with different concentrations of free DOX (0.97, 1.3, and 1.95 μM) and measured the cell viability at 1 day after treatements, as shown in Figure 5b. Compared with DOX-loaded PLGA−Au H-S NPs containing same quantity of doxorubicin, free DOX resulted in the lower viability due to a sustained release of DOX from PLGA NPs.

The amount of heat induced upon NIR irradiation depends upon the NIR intensity and irradiation time, as well as upon the NP concentration. Therefore, we fixed the NIR intensity at 0.7 W/cm^2 and investigated the influence of NIR irradiation times and NP concentrations on the viability of HeLa cells treated with PLGA−Au H-S NPs to investigate the effect of photothermal treatment. Figure 5c shows the cell viability of HeLa cells incubated with 120 μg/cm^2 PLGA H-S NPs for 4 h and then irradiated by 0.7 W/cm^2 NIR for different lengths of time. The cell viability decreased, as the NIR exposure time increased, particularly when the cells were exposed to NIR light for longer than 6 min; at this time period, the viability was reduced to below 20%. Because the temperature of the medium was raised to about 43 and 44 °C by 5 and 6 min-NIR irradiation, respectively, the HeLa cells were considered to be significantly damaged above 44 °C.

To see if the damage caused by NIR irradiation was reversible or irreversible, we also measured cell viability at various times after NIR irradiation for HeLa cells incubated with different concentrations of PLGA−Au H-S NPs (60, 120, and 180 μg/cm^2) for 4 h and irradiated by 0.7 W/cm^2 NIR for 4 min (Figure 5d). After NIR irradiation, the cells were incu-

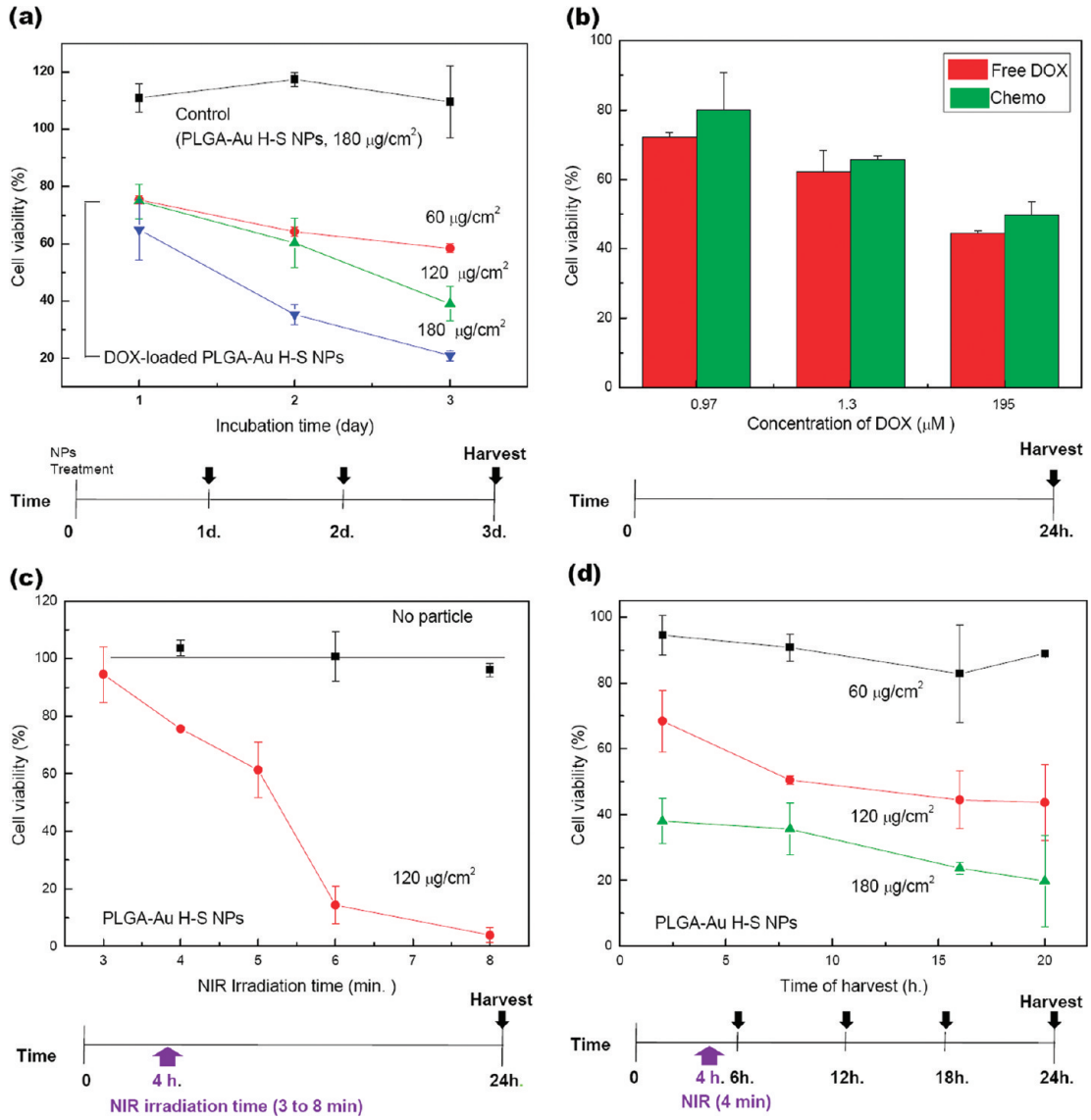

Figure 5. (a) Cell viability *versus* incubation time for HeLa cells treated with different concentrations of DOX-loaded PLGA−Au H-S NPs. The results of HeLa cells treated with PLGA−Au H-S NPs are included as a control. (b) Cell viability for HeLa cells treated with different concentrations of free DOX and DOX-loaded PLGA−Au H-S NPs containing same quantity of doxorubicin (0.97, 1.3, and 1.95 μM). (c) Cell viability *versus* NIR irradiation time for HeLa cells treated with 120 μg/cm² PLGA−Au H-S NPs. The results of untreated HeLa cells are included as a control. (d) Cell viability *versus* additional incubation time for HeLa cells incubated with different concentrations of PLGA−Au H-S NPs for 4 h, irradiated with 0.7 W/cm² NIR for 4 min, and then further incubated before measuring viability.

bated again at 37 °C before measuring the viability. At 60 μg/cm², the cell viability decreased to about 80% at 14 h, but increased back to about 90% during the next 6 h. For 120 and 180 μg/cm², however, the cell viability decreased continuously with time. Because the temperature of the medium increased to about 40, 42, and 47 °C upon NIR exposure for 60, 120, and 180 μg/cm², respectively, these results suggest that a high dose of heat led to irreversible damage to the cells, whereas the reduced viability induced by the low dose of heat was recoverable. In these experiments, we used 96-well plates with a well diameter of 6.38 mm. Because the beam diameter of NIR light was about 6 mm, we assumed that most of the cells in the well were exposed to NIR light.

For combined doxorubicin and photothermal treatment, we incubated HeLa cells with different concentrations of DOX-loaded PLGA−Au H-S NPs for 4 h and irradiated them with 0.7 W/cm² NIR for 4 min. Subsequently, we incubated them again for 20 h and then measured their viability using CCK-8 (Figure 6a). As expected from the results obtained using the calcein-AM assay, the chemo-photothermal treatments resulted in lower viabilities than did chemo- or photothermal treatment alone. Moreover, the combined treatments shortened the time required to decrease the cell viability below 50%.

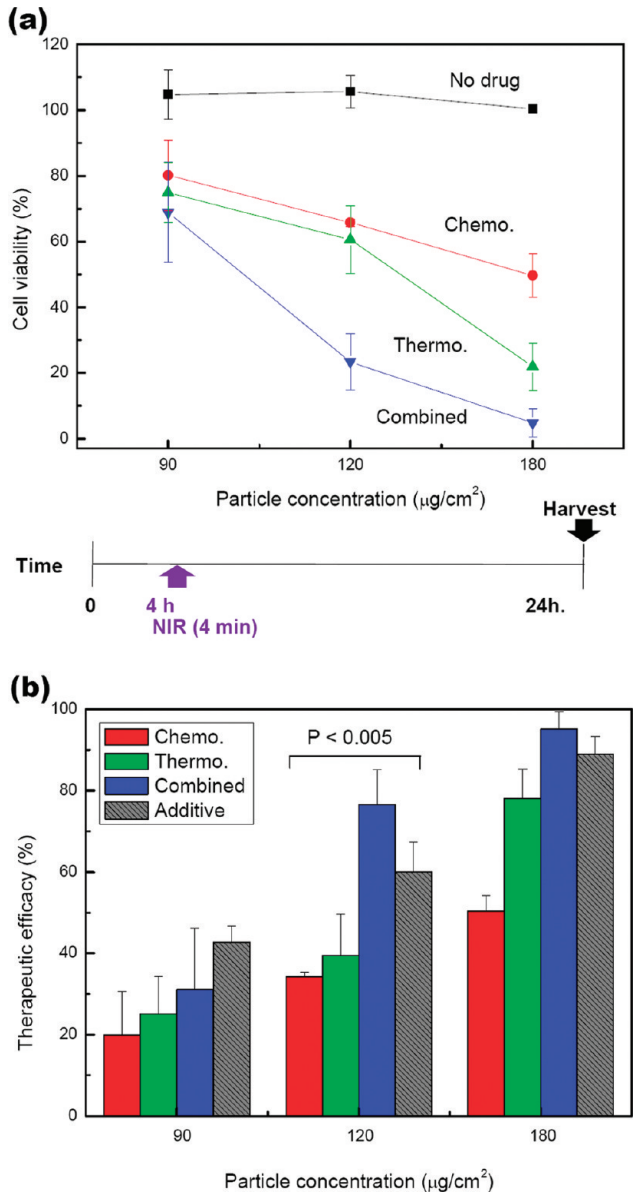

Figure 6. (a) Comparison of cell viability following chemo, photothermal, chemo-photothermal treatments. (b) Therapeutic efficacy *versus* NP concentration for different treatments. Therapeutic efficacy was calculated by subtracting cell viability from 100%. Additive therapeutic efficacies of chemo and photothermal treatments were estimated using the relation of $T_{addiive} = 100 - (f_{chemo} \times f_{photothermal}) \times 100$, where *f* is the fraction of surviving cells after each treatment. When the efficacy of combined treatment is compared with the efficacies of chemo- and photothermal treatments and the additive value using *t* test, p-value is lower than 0.005.

The viability of cells treated with 120 μg/cm² DOX-loaded PLGA−Au H-S NPs decreased to about 40% in 3 d without NIR irradiation (Figure 5a). However, when the cells treated with 120 μg/cm² DOX-loaded PLGA−Au H-S NPs were exposed to 0.7 W/cm² NIR for 4 min, the cell viability was reduced to about 20% in only one day (Figure 6a). In Figure 6b, the therapeutic efficacies calculated by subtracting the cell viability from 100% are compared with the additive therapeutic efficacies of chemo- and photothermal treatments, which were estimated using the relation of $T_{addiive} = 100 - (f_{chemo} \times f_{photothermal}) \times 100$, where *f* is the fraction of surviving cells after each treatment.[8] For 120 and 180 μg/cm², the measured therapeutic efficacy of chemo-photothermal therapy was higher than the additive therapeutic efficacy of chemo- and photothermal therapy, demonstrating the synergistic effect of chemo-photothermal treatment.

CONCLUSION

In summary, we fabricated DOX-loaded PLGA−Au H-S NPs that can deliver both drug and heat simultaneously to a selected tumorigenic region. When NPs were incubated with HeLa cells, they were endocytosed and accumulated within vesicles and organelles. Furthermore, drug loaded in PLGA NPs was released more rapidly upon NIR irradiation, confirming the occurrence of photothermally controlled drug delivery. To investigate the therapeutic effects of chemo-photothermal treatment, we mesured the cell viability using calcein-AM and CCK-8 assays of HeLa cells treated with DOX-loaded PLGA−Au H-S NPs and then irradiated with NIR light. Compared with chemo- and photothermal treatment alone, the combined treatment yielded higher cytotoxicity, which was greater than the sum of the independent treatments, thus demonstrating a synergistic effect. Furthermore, the treatment time was decreased by the combined treatment. For HeLa cells treated with DOX-loaded PLGA−Au H-S NPs, but not irradiated by NIR light, viability decreased slowly due to the sustained release of doxorubicin from PLGA NPs. However, once the treated cells were exposed to NIR light, viability decreased rapidly. In these *in vitro* studies, the NPs were not conjugated with targeting ligands, because it is difficult to quantify the number of targeted NPs in the cells (which influences the amount of heat) if the conjugated NPs are targeted to specific cells and then washed out. However, if these NPs were to be conjugated with targeting ligands, as reported previously,[28] selective cell targeting might be possible.

METHODS

Preparation and Characterization of DOX-Loaded PLGA NPs. PLGA (100 mg, M_w = 20000 or 5000, Wako Chemicals) and doxorubicin (2 mg, M_w = 579, Fluka) or rhodamine B (4 mg, M_w = 443, Sigma-Aldrich) were dissolved in a 50:50 ratio in 10 mL of chloroform. The organic solution was mixed with 20 mL of aqueous phase containing poly (vinyl alcohol) (2%, molecular weight = 15000−20000, Aldrich Chemical Co.) as a stabilizer. After mutual saturation of the organic and continuous phases, the mixture was emulsified for 10 min by ultrasonication at 250 W. The organic solvent was evaporated and the DOX-loaded PLGA NPs were purified by centrifugation at 2 × 10⁴ rpm for 30 min. The size of the NPs, determined by dynamic light scattering (DLS), was ap-

proximately 75 ± 12 nm in diameter, and their glass transition temperatures measured by differential scanning calorimetry (TA Instrument, SDT-600) were about 43 and 38 °C for PLGA NPs of M_w 20000 and 5000, respectively.

The amount of encapsulated doxorubicin was measured as follows. The mass of the dried DOX-loaded PLGA NPs was measured and the NPs were dissolved in dimethyl sulfoxide (Alrich Chemical Co.) to extract doxorubicin from the NPs. Then, the amount of doxorubicin was measured using a UV spectrometer (Optizen 2120UV, Mecasys Co.). The loading efficiency, which is defined as the percentage of the actual mass of doxorubicin loaded in the PLGA NPs relative to the mass of the PLGA NPs, was estimated to be about 1.9%.

Fabrication of DOX-Loaded PLGA−Au H-S NPs. DOX-loaded PLGA−Au H-S NPs were fabricated by depositing 15-nm-thick Au layers onto monolayers of DOX-loaded PLGA NPs, which were prepared by spin-casting aqueous suspensions of NPs on a silicon substrate, as reported by H. Park *et al.*[24] After depositing the Au film, Au-deposited DOX-loaded PLGA NPs were released into water from the substrate surface by sonication and then collected by centrifugation. The absorption peak of these DOX-loaded PLGA−Au H-S NPs was measured with a UV−visible/NIR spectrometer, and was about 810 nm.

***In Vitro* Release Experiments.** A 2 ml portion of DOX-loaded PLGA−Au H-S NPs solution with concentration of about 200 μg/mL was loaded into a 1000 Da molecular weight cutoff membrane dialysis tube. The tube was immersed in a transparent vial filled with 5 mL of phosphate buffer solution (pH 7.4, 10 mM) during release experiments. The release experiments were performed with and without NIR 4 min irradiation at initial time of experiment at 37 °C. The amount of released DOX was measured through UV absorbance. All measurements were conducted in triplicate.

Cell Cultures. The HeLa human cervical cancer cell line was seeded onto 6-well or 96-well plates, or coverglass-bottom dishes, with growth areas of 9.6, 0.32, or 1.13 cm^2, respectively, depending upon the experiment. Then, the cells were cultured in Dulbecco's modified essential medium (DMEM) (Sigma-Aldrich) supplemented with 10% fetal bovine serum at 37 °C with 5% CO_2 for 24 h. Next, the medium was removed and the medium containing DOX-loaded PLGA−Au H-S NPs or PLGA−Au H-S NPs was added, and the cells were incubated for specific lengths of time, as indicated in the text.

Transmission Electron Microscopy (TEM). HeLa cells (5×10^5) were seeded onto 6-well plates and incubated in 3 mL of medium with PLGA−Au H-S NPs (30 μg/cm^2) for ~4 to 12 h. Then, the cells were rinsed three times with phosphate buffered saline (PBS) and a cell pellet was collected using trypsin-EDTA and centrifugation. For TEM analysis, ultrathin (80 nm) sections of the cell pellet were prepared by a standard method, as described by D. R. Rowley *et al.*[29] The samples were examined using TEM (JEM-1011, JEOL).

Confocal Microscopy. HeLa cells (1×10^4) were seeded onto a coverglass-bottom dish (1.13 cm^2) and incubated in 200 μL of the medium with rhodamine-loaded PLGA−Au H-S NPs (17.5 μg/cm^2) at 37 °C in 5% CO_2 for 12 h. Then, the medium was replaced with fresh medium without NPs and the dish was transferred to a laser scanning confocal microscope (UltraVIEW RS, PerkinElmer) equipped with an incubator set at 37 °C with 5% CO_2. Every 30 min, a florescence image was obtained at a fixed focal plane while the cells were exposed to continuous NIR light of power 0.7 W/cm^2 using a 808-nm coherent diode laser (Unique mode 30k/400/20, 808 ± 3 nm, Jenoptik Co.). Similar images were also measured without NIR irradiation. The cells were stained with wheat germ agglutinin, which is a marker protein for the surface membrane of cells (Invitrogen).

Cell Viability Evaluation of *in Vitro* Chemo, Photothermal, and Chemo-Photothermal Treatments Using Calcein-AM Assay. HeLa cells (5×10^4) were seeded onto a coverglass-bottom dish and incubated in 200 μL of the medium with PLGA−Au H-S NPs or DOX-loaded PLGA−Au H-S NPs (70.9 μg/cm^2) at 37 °C with 5% CO_2 for 24 h. Then, the cells were irradiated with 0.7 W/cm^2 NIR light for 10 min for photothermal and chemo-photothermal treatments, whereas for chemotherapy alone, the cells were not exposed to NIR light. After treatment, the cells were stained with 1 μM calcein-AM and cell viability was estimated with a fluorescence optical microscope (Leica DM 2500, Leica).

Cell Viability Evaluation of *in Vitro* Chemo, Photothermal, and Chemo-Photothermal Treatments Using CCK-8 Assay. HeLa cells (8×10^3) were seeded onto 96-well plates and incubated in 200 μL of medium with PLGA−Au H-S NPs or DOX-loaded PLGA−Au H-S NPs (60, 120, or 180 μg/cm^2). At 4 h after incubation, the cells were exposed to 0.7 W/cm^2 NIR light for 4 min (except for Figure 3b) for photothermal and chemo-phothermal treatments, and then incubated again at 37 °C with 5% CO_2 for specific lengths of time, as indicated in the text. After treatment, 10 μL of the CCK-8 solution was added to each well of the plate, followed by incubation for another 1−3 h. Then, cell viability was determined by measuring absorbance at the wavelength of 450 nm with a microplate reader. All of the measurements were conducted in triplicate.

Acknowledgment. This work has been financially supported by Korea Science and Engineering Foundation through National Core Research Center for Nanomedical Technology (Grant No. R15-20040924-00000-0).

REFERENCES AND NOTES

1. Arcamene, F.; Franceschi, G.; Penco, S.; Selva, A. Adriamycin (14-Hydroxydaunorubicin), a Novel Antitumor Antibiotic. *Tetrahedron Lett.* **1969**, *13*, 1007–1010.
2. Umezawa, H.; Maeda, K.; Takauchi, T.; Okami, Y. New Antibiotics, Bleomycin A and B. *J. Antibiot.* **1966**, *A19*, 200–209.
3. Donaldson, K. L.; Goolsby, G. L.; Wahl, A. F. Cytotoxicity of the Anticancer Agents Cisplatin and Taxol during Cell Proliferation and the Cell Cycle. *Int. J. Cancer.* **1994**, *57*, 847–55.
4. Farokhzad, O. C.; Langer, R. Impact of Nanotechnology on Drug. *ACS Nano* **2009**, *3*, 16–20, and references therein.
5. Tannock, I. F. Treatment of Cancer with Radiation and Drugs. *J. Clin. Oncol.* **1996**, *14*, 3156–3174.
6. Hassan, M. A. E.; Mastenbroek, D.; Gerritsen, W.; Giaccone, G.; Kruyt, F. Overexpression of Bcl2 Abrogates Chemo- And Radiotherapy-Induced Sensitisation of NCI-H460 Non-small-Cell Lung Cancer Cells to Adenovirus-Mediated Expression of Full-Length TRAIL. *Br. J. Cancer.* **2004**, *91*, 171–177.
7. Saad, M.; Garbuzenko, O. B.; Minko, T. Co-delivery of siRNA and an anticancer drug for treatment of multidrug-resistant cancer. *Nanomedicine.* **2008**, *3*, 761–776.
8. Hahn, G. M.; Braun, J.; Har-kedar, I. Thermochemotherapy: Synergism between Hyperthermia (42−43o) and Adriamycin (or Bleomycin) in Mammalian Cell Inactivation. *Proc. Nat. Acad. Sci U.S.A.* **1975**, *72*, 937–940.
9. Overgaard, J. Combined Adriamycin and Hyperthermia Treatment of a Murine Mammary Carcinoma *in Vivo*. *Cancer Res.* **1976**, *36*, 3077–3081.
10. Johnson, H. A.; Pavelec, M. Thermal Enhancement of Thio-Tepa Cytotoxity. *J. Natl. Cancer Inst.* **1973**, *50*, 903–908.
11. Eikesdal, H. P.; Bjerkvig, R.; Raleigh, J. A.; Mella, O.; Dahl, O. Tumor Vasculature Is Targeted by the Combination of Combretastatin A-4 and Hyperthermia. *Radiother. Oncol.* **2001**, *61*, 313–320.
12. Nelson, B. K.; Conover, D. L.; Krieg, E. F., Jr.; Snyder, D. L.; Edwards, R. M. Interactions of Radiofrequency Radiation-Induced Hyperthermia and 2-Methoxyethanol Teratogenicity in Rats. *Bioelectromagnetics* **1997**, *18*, 349–359.
13. Diederich, C. J.; Hynynen, K. Ultrasound Technology for Hyperthermia. *Ultrasound Med. Biol.* **1999**, *25*, 871–887.
14. Loo, C.; Lowery, A.; Halas, N.; West, J.; Drezek, R. Immunotargeted Nanoshells for Integrated Cancer Imaging and therapy. *Nano Lett.* **2005**, *5*, 709–711.
15. Hirsh, L. R.; Stafford, R. J.; Bankson, J. A.; Sersher, S. R.; Rivera, B. R.; Price, E.; Hazle, J. D.; Halas, N. J.; West, J. L. Nanoshell-Mediated near-Infrared Thermal Therapy of Tumors under Magnetic Resonance Guidance. *Proc. Natl. Acad. Sci. U.S.A.* **2003**, *100*, 13549–13554.

16. Sershen, S. R.; Westcott, S. L.; Halas, N. J.; West, J. L. Temperature-Sensitive Polymer-Nanoshell Composites for Photothermally Modulated Drug Delivery. *J. Biomed. Mater. Res.* **2000**, *51*, 293–298.
17. Chen, J.; Saeki, F.; Wiley, B. J.; Chang, H.; Cobb, M. J.; Li, Z.-Y.; Au, L.; Zhang, H.; Kimmey, M. B.; Li, X.; Xia, Y. Gold Nanocages: Bioconjugation and Their Potential Use as Optical Imaging Contrast Agents. *Nano Lett.* **2005**, *5*, 473–477.
18. Chen, J.; Wang, D.; Xi, J.; Au, L.; Siekkinen, A.; Warsen, A.; Li, Z.-Y.; Zhang, H.; Xia, Y.; Li, X. Immuno Gold Nanocages with Tailored Optical Properties for Targeted Photothermal Destruction of Cancer Cells. *Nano Lett.* **2007**, *7*, 1318–1322.
19. Huang, X.; El-Sayed, I. H.; Qian, W. M.; El-Sayed, A. Cancer Cell Imaging and Photothermal Therapy in the Near-Infrared Region by Using Gold Nanorods. *J. Am. Chem. Soc.* **2006**, *128*, 2115–2120.
20. Tong, L.; Zhao, Y.; Huff, T. B.; Hansen, M. N.; Wei, A.; Cheng, J.-X. Gold Nanorods Mediate Tumor Cell Death by Compromising Membrane Integrity. *Adv. Mater.* **2007**, *19*, 3136–3141.
21. Kam, N. W. S.; O'Connell, M.; Wisdom, J. A.; Dai, H. Carbon Nanotubes As Multifunctional Biological Transporters and near-Infrared Agents for Selective Cancer Cell Destruction. *Proc. Natl. Acad. Sci. U.S.A.* **2005**, *102*, 11600–11605.
22. Zimmerman, N. S.; Swafford, A. D.-E.; Bajaj, P.; Musselman, I. H.; Pantano, P.; Draper, R. K.; Vitetta, E. S. Thermal Ablation of Tumor Cells with Antibody-Functionalized Single-Walled Carbon Nanotubes. *Proc. Natl. Acad. Sci. U.S.A.* **2008**, *105*, 8697–8702.
23. Hauck, T. S.; Jennings, T. L.; Yatsenko, T.; Kumaradas, J. C.; Chan, W. C. W. Enhancing the Toxicity of Cancer Chemotherapeutics with Gold Nanorod Hyperthermia. *Adv. Mater.* **2008**, *20*, 3832–3838.
24. Park, H.; Yang, J.; Seo, B.; Kim, K.; Suh, J.; Kim, D.; Haam, S.; Yoo, K.-H. Multifuctional Nanoparticles for Photothermally Controlled Drug Delivery and Magnetic Resonance Imaging Enhancement. *Small.* **2008**, *4*, 192–196.
25. The treated particle concentration. 100, 150, 200, 300 μg/mL × 200 μl/0.32 cm^2 ≈ 60, 90, 120, 180 μg/cm^2
26. Zolink, B. S.; Leary, P. E.; Burgess, D. J. Elevated Temperature Accelerated Release Testing of PLGA Microspheres. *J. Controlled Release* **2006**, *112*, 293–300.
27. McConnell, H. M.; Hubbell, W. L. Molecular Motion in Spin-Labeled Phospholipids and Membranes. *J. Am. Chem. Soc.* **1971**, *93*, 314–326.
28. Lee, J.; Yang, J.; Ko, H.; Oh, S. J.; Kang, J.; Son, J.-H.; Lee, K.; Lee, S.-W.; Yoon, H.-G.; Suh, J.-S.; *et al.* Multifunctional Magnetic Gold Nanocomposites: Human Epitherial Cancer Detection *via* Magnetic Resonance Imaging and Localized Synchronous Therapy. *Adv. Funct. Mater.* **2008**, *18*, 258–264.
29. Rowley, D. R.; Feuchter, F. A.; Heidger, P. M. Cell Culture Method for Facilitating Preparations for Electron Microscopy and Replicate Sampling Using Aclar Fluoroplastic. *Methods Cell Sci.* **1979**, *5*, 1067–1069.